

Three-qubit Parity Gate via Simultaneous Cross Resonance Drives

Toshinari Itoko,^{1,*} Moein Malekakhlagh,² Naoki Kanazawa,¹ and Maika Takita²

¹IBM Quantum, IBM Research – Tokyo, Tokyo, Japan

²IBM Quantum, IBM Thomas J. Watson Research Center, Yorktown Heights, NY 10598

(Dated: October 6, 2023)

Native multi-qubit parity gates have various potential quantum computing applications, such as entanglement creation, logical state encoding and parity measurement in quantum error correction. Here, using simultaneous cross-resonance drives on two control qubits with a common target, we demonstrate an efficient implementation of a three-qubit parity gate. We have developed a calibration procedure based on the one for the echoed cross-resonance gate. We confirm that our use of simultaneous drives leads to higher interleaved randomized benchmarking fidelities than a naive implementation with two consecutive CNOT gates. We also demonstrate that our simultaneous parity gates can significantly improve the parity measurement error probability for the heavy-hexagon code on an IBM Quantum processor using seven superconducting qubits with all-microwave control.

I. INTRODUCTION

Standard implementation of quantum computing [1, 2] involves expressing multi-qubit operations in terms of a universal set of single- and two-qubit gates [3]. Through quantum circuit optimization, one can achieve an equivalent shallower-depth circuit, benefiting not only from less incoherent error, caused by energy relaxation and dephasing [4–6], but also possibly from less coherent (control) error. At a high level, strategies for circuit optimization can be software- [7–11] and/or hardware-inspired [12–20]: the former employs unitary group identities for simplification, while the latter considers the hardware connectivity, and explores the hardware potential to achieve more efficient two- or multi-qubit gates. Here, following the latter approach, and inspired by Cross-Resonance (CR) [21–25] quantum processors provided by IBM, we study a Three-qubit Parity (TP) gate [26], and provide an efficient calibration based on the existing Echoed Cross-Resonance (ECR) scheme [25, 27–30].

Having efficient parity gates [31, 32] in the native gate set is useful for numerous applications. In particular, the utility of a TP gate boils down to its local equivalence with two consecutive CNOTs (Two-CX) on three qubits, in which they share either a common control (or target) qubit [Fig. 1(a)]. Such a circuit subroutine appears for instance in (i) the creation of multi-qubit entanglement, in particular the Greenberger-Horne-Zeilinger (GHZ) state [33, 34], (ii) logical encoder and parity check syndrome measurement in Quantum Error Correction (QEC) [35–37], and (iii) successive swaps across a qubit network [38, 39].

In this paper, we present a TP gate implementation that fits well with IBM’s CR architecture. Our implementation closely follows that of the ECR gate [25, 28, 29, 40], but instead employs two simultaneous CR drives with a common target qubit, hence named Simultaneous Cross Resonance Parity (SCR P) gate [Fig. 1(b)–

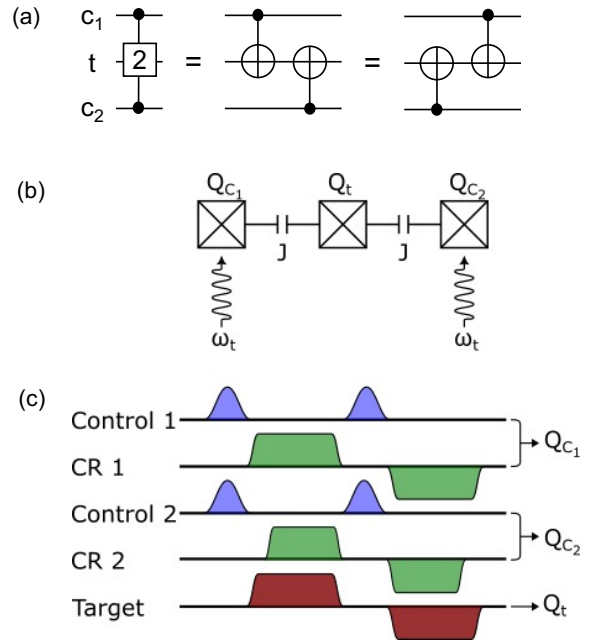


FIG. 1. **Implementation of three-qubit parity gate with simultaneous CR drives.** (a) Circuit representation of a Z -parity gate, equivalent to two consecutive CNOTs with a common target. The case with a common control is locally equivalent up to single-qubit Hadamard gates. (b) Cross-resonance schematics with two control (c_1 and c_2) and one target (t) qubits. (c) Pulse-level implementation using simultaneous CR drives following the ECR calibration [25, 27–30]. The CR (green) and rotary (red) pulses have a carrier frequency resonant with the target qubit.

(c)]. This protocol implements a three-qubit Z -parity gate, which is locally equivalent to any other TP gates. Our use of simultaneous drives should work in principle if each CR pulse leads only to a ZX interaction between the intended qubits. In other words, SCR P gives ZXI and IXZ interactions [41], that are commutative, hence additive. Intuitively, the SCR P implementation should improve the fidelity of the Z -parity gate mainly due to its

* itoko@jp.ibm.com

shorter pulse schedule. We confirm that unwanted cross-drive contributions are indeed higher-order effects, and hence weaker, by deriving an effective three-qubit gate Hamiltonian using Schrieffer-Wolff Perturbation Theory (SWPT) [24, 25, 42–45] (Sec. II). Using Interleaved Randomized Benchmarking (IRB) [46–49], we demonstrate improved Error Per Gate (EPG) for the SCRП implementation compared to Two-CX. Furthermore, we demonstrate the SCRП implementation improves the fidelity of parity measurement on an IBM Quantum processor [50], namely `ibm_auckland`. In particular, the SCRП implementation can reduce the average syndrome error probability of X -parity measurement for the heavy-hexagon code [51–53] by up to 28 percents comparing with a naive implementation with CNOT gates on the device (Sec. IV).

The rest of this paper is organized as follows: first, in Sec. II, we study effective gate interactions for the SCRП gate implementation using SWPT. In Sec. III, we discuss the SCRП calibration of the TP gate, and provide IRB results that demonstrate improvement in EPG with respect to the standard Two-CX implementation. Furthermore, in Sec. IV, We showcase the SCRП gate’s utility in improving the syndrome measurement success probability of the heavy-hexagon code. Finally, Sec. V concludes the paper, and examines further potential applications and extensions of the SCRП idea.

II. HAMILTONIAN ANALYSIS

We next provide a Hamiltonian analysis for the SCRП gate, based on SWPT [24, 25, 43]. Our analysis clarifies why the SCRП gate works in practice: at sufficiently weak CR drive, the effective ZXI and IXZ rates depend only on their corresponding drive amplitudes. Furthermore, undesired three-qubit cross interactions such as the ZXZ term appears only at higher order, and hence are weaker.

We model the transmon qubits as a set of Duffing oscillators with nearest-neighbor exchange interaction under Rotating-Wave Approximation (RWA) as:

$$\hat{H}_s = \sum_{j=c_1, c_2, t} \left(\omega_j \hat{a}_j^\dagger \hat{a}_j + \frac{\alpha_j}{2} \hat{a}_j^\dagger \hat{a}_j^\dagger \hat{a}_j \hat{a}_j \right) + \sum_{\langle j, k \rangle} J_{jk} \left(\hat{a}_j^\dagger \hat{a}_k + \hat{a}_j \hat{a}_k^\dagger \right), \quad (1)$$

with ω_j , α_j and J_{jk} as the qubit frequency, anharmonicity, and pairwise exchange interaction, respectively, for $j, k \in \{c_1, c_2, t\}$. Furthermore, we model the CR and a possible direct target drives as

$$\hat{H}_d(t) = \sum_{j=c_1, c_2, t} \frac{1}{2} \left[\Omega_j^*(t) e^{i\omega_d t} \hat{a}_j + \Omega_j(t) e^{-i\omega_d t} \hat{a}_j^\dagger \right], \quad (2)$$

with $\Omega_j(t) \equiv \Omega_{jX}(t) + i\Omega_{jY}(t)$ and ω_d denoting the complex-valued envelope and the common carrier frequency, respectively. In the rotating frame (RF) of the

drive, which is set to the target qubit frequency, the Hamiltonian simplifies to:

$$\begin{aligned} \hat{H}_{\text{rf}}(t) \equiv & \sum_{j=c_1, c_2, t} \left(\Delta_{jd} \hat{a}_j^\dagger \hat{a}_j + \frac{\alpha_j}{2} \hat{a}_j^\dagger \hat{a}_j^\dagger \hat{a}_j \hat{a}_j \right) \\ & + \sum_{\langle j, k \rangle} J_{jk} \left(\hat{a}_j^\dagger \hat{a}_k + \hat{a}_j \hat{a}_k^\dagger \right) \\ & + \sum_{j=c_1, c_2, t} \frac{1}{2} \left[\Omega_j^*(t) \hat{a}_j + \Omega_j(t) \hat{a}_j^\dagger \right]. \end{aligned} \quad (3)$$

where $\Delta_{jd} \equiv \omega_j - \omega_d$. The RF Hamiltonian (3) is the starting point of our analysis. To understand the SCRП power budget, for simplicity, we assume an always-on X-quadrature-only CW drive $\Omega_j(t) = \Omega_j$.

Applying time-independent SWPT, we derive effective (resonant) interactions for the SCRП gate through recursive frame transformations that averages over off-resonant transitions [24, 25, 43]. The relevant SCRП frame is diagonal with respect to the two control qubits, i.e. allowing only I and Z on the controls, and off-diagonal with respect to the target. We treat the first two lines of Eq. (3) as the bare, and the last line as the interaction Hamiltonian.

Up to the zeroth order, the exchange interaction leads to nearest-neighbor static ZZ interactions:

$$\omega_{ZZI}^{(0)} = \frac{J_{c_1 t}^2}{\Delta_{c_1 t} - \alpha_t} - \frac{J_{c_1 t}^2}{\Delta_{c_1 t} + \alpha_{c_1}}, \quad (4)$$

$$\omega_{IZZ}^{(0)} = \frac{J_{c_2 t}^2}{\Delta_{c_2 t} - \alpha_{c_2}} - \frac{J_{c_2 t}^2}{\Delta_{c_2 t} + \alpha_{c_2}}. \quad (5)$$

Up to the dominant (linear) order in drive amplitudes, the ZXI and IXZ terms are independent, i.e. no cross-drive exists, justifying why such a simultaneous calibration works:

$$\omega_{ZXI}^{(1)} = -\frac{J_{c_1 t} \alpha_{c_1}}{\Delta_{c_1 t} (\Delta_{c_1 t} + \alpha_{c_1})} \Omega_{c_1}, \quad (6)$$

$$\omega_{IXZ}^{(1)} = -\frac{J_{c_2 t} \alpha_{c_2}}{\Delta_{c_2 t} (\Delta_{c_2 t} + \alpha_{c_2})} \Omega_{c_2}, \quad (7)$$

$$\omega_{IXI}^{(1)} = \Omega_t - \frac{J_{c_1 t}}{\Delta_{c_1 t} + \alpha_{c_1}} \Omega_{c_1} - \frac{J_{c_2 t}}{\Delta_{c_2 t} + \alpha_{c_2}} \Omega_{c_2}. \quad (8)$$

At second, and higher-order in drive amplitudes, we find cross-drive contributions to the Stark shifts, ZZI and IZZ rates, as well as to ZXI , IXZ and ZXZ terms.

Based on Eqs. (6)-(7), the cross-drive-free nature of the desired ZXI and IXZ rates up to the leading order allows us to employ the existing CR echo calibration [25, 27–30] in constructing the SCRП gate. In particular, the CR echo sequence removes the IXI term, and suppresses the dominant error terms ZZI and IZZ up to the leading order. We discuss the SCRП calibration in more detail in the following section.

III. PARITY GATE CALIBRATION

Our SCRП pulse schedule for implementing a three-qubit Z -parity gate is shown in Fig. 1(c), which is inspired by the CR echo calibration for a CNOT gate [27, 28]. The main part (green) consists of two echoed sequences of simultaneous CR drives onto the control qubits c_1 and c_2 with the carrier frequencies set to the target qubit frequency. Moreover, interleaving X_π pulses (purple) onto the control qubits c_1 and c_2 allows for echoing out nearest-neighbor ZZ (i.e. ZZI and IZZ), as well as the IXI Hamiltonian terms up to the leading order [25, 30]. Each individual CR echo calibration may also be accompanied with simultaneous resonant rotary tones onto the target qubit t (shown altogether in red) [30]. The rotary tones were designed to suppress several unwanted terms in the effective Hamiltonian of the echoed CR drives, namely the Y error on the target as well as target-spectator crosstalk [30]. To implement a Z -parity gate, three additional local Clifford instructions are needed in front (or back) of the schedule; namely $Z_{\pi/2}$ on c_1 and c_2 , and X_π on t .

We have developed a straightforward calibration procedure for the Z -parity gate based on the well-established CR echo calibration for CNOT gates [27, 28], where we adopt the two CR echo pulse configurations, i.e. amplitudes and angles, while we replace the independently calibrated rotary tones with a simultaneous SCRП rotary tone. For example, to implement a Z -parity gate on qubits (0, 1, 2), we use pulse amplitudes and angles calibrated for CR(0, 1) and CR(2, 1) as those for two echoed CR pulses to drive simultaneously. We place two echoed CR sequences so that their X_π pulses in center are aligned as shown in Fig. 1(c). Note that we could recalibrate those CR pulses at once so that they have the same duration and the resulting rotation in the target qubit becomes the desired angle for any binary input to the two control qubits, i.e. π for 00, $-\pi$ for 11, and 0 for 01 and 10. However, for simplicity, we reuse CR pulse configurations for two-qubit gates to implement SCRП gates in all experiments we conduct hereafter. To calibrate the simultaneous rotary tone in our SCRП implementation, we adopt and generalize the Hamiltonian Error Amplifying Tomography (HEAT) technique [30] (See Appendix 1).

We characterize the potential improvement by the SCRП implementation in the fidelity of a Z -parity gate by comparing it with a naive implementation with two consecutive CNOT gates using IRB [49]. We prepare two interleaved sequences from a common reference Clifford sequence. Both interleave a Z -parity gate, but with different implementations: one implemented with SCRП and the other implemented with two CNOT gates (See Appendix 2). We conducted such an IRB experiment using qubits (8, 11, 14) on `ibm_auckland`. We used ten Clifford lengths: 2, 3, 4, 5, 7, 9, 12, 17, 25, 38. For each Clifford length, we sampled 50 RB circuits and computed survival rate from 400 shots for each circuit. We fit an exponential curve to the averaged survival rates (over the

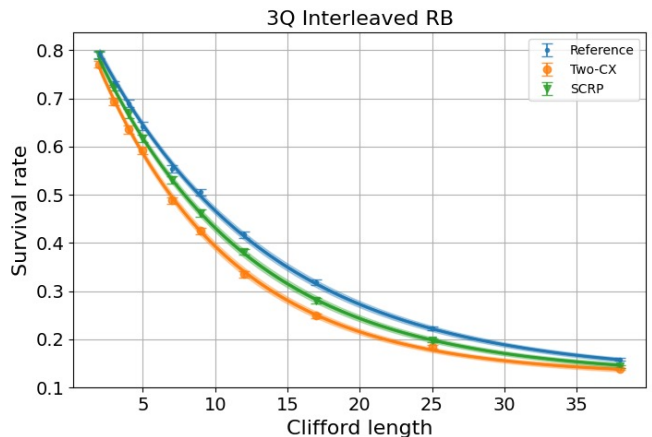


FIG. 2. Interleaved RB comparing two Z -parity gate implementations, the consecutive two CNOT gates (Two-CX, orange) and the simultaneous CR drives (SCRП, green) on qubits (8, 11, 14) on `ibm_auckland`. The estimated EPGs are 0.02109 ± 0.00105 (Two-CX) and 0.00964 ± 0.00095 (SCRП).

IRB seeds and shots) [49].

Figure 2 shows the result obtained from the IRB experiment. It contains three decay curves corresponding to a reference sequence (blue), interleaved SCRП implementation (green), and interleaved Two-CX implementation (orange) of the Z -parity gate, respectively. The decay curve of SCRП appears clearly higher than that of Two-CX, suggesting a higher gate fidelity. For reference, the EPG estimated by the ratio of decay rates (the reference and the sequence of interest) was improved from 0.02109 ± 0.00105 (Two-CX) to 0.00964 ± 0.00095 (SCRП). This improvement is in part owed to the reduction in the gate length from 704.0 ns (Two-CX) to 369.8 ns (SCRП). Estimating best possible average gate error based on the coherence limit [54, 55], we find the limits as 0.0122 (Two-CX) and 0.00645 (SCRП). These coherence limits are calculated from the gate lengths, T_1 values of (122.7, 134.8, 159.7) μ s, and T_2 values of (73.4, 111.4, 170.3) μ s, for `ibm_auckland` qubits (8, 11, 14), respectively (See Appendix 3).

IV. EXPERIMENTS

We next demonstrate how the SCRП calibration improves the fidelity of parity measurement for QEC on IBM devices. Here, we focus on the X -parity measurement of the heavy-hexagon code [40, 51, 56]. The circuit realization requires seven qubits, consisting of four data qubits (D1–D4; gray), two flag qubits (F1 and F2; white) and one syndrome qubit (S; black), with a connectivity with degree at most three, as shown in Fig. 3(a). The standard X -parity check circuit is originally represented with eight CNOT gates as shown in Fig. 3(b). It consists of four pairs of two CNOT gates with a common control and distinct target qubits, i.e. X -parity gates,

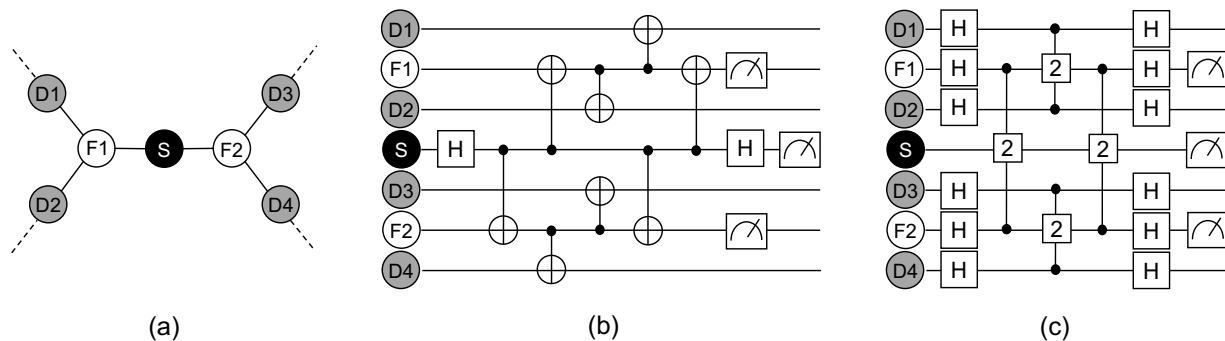


FIG. 3. **X-Parity measurement circuit for heavy-hexagon code.** (a) 7-qubit subsystem of interest. (b) Original representation with CNOT gates [51]. (c) Representation with Z -parity gates useful for SCR implementation, which reduces the circuit depth by a factor of approximately 3/5, and uses only 4 SCR gates compared to 8 CNOT gates.

which are locally equivalent to Z -parity gates up to a change of basis using single-qubit hadamard gates. Applying the replacement, the X -parity check circuit will have an efficient representation with just four Z -parity gates as shown in Fig. 3(c). We used the latter circuit representation and compared the (i) Two-CX, and (ii) SCR implementations of the Z -parity gates.

The `ibm_auckland` processor has 27 qubits, from which we used qubits (5, 8, 9, 11, 13, 14, 16) ordered as (D1, F1, D2, S, D3, F2, D4). Qubit transition frequencies ($\omega_{01}/2\pi$) of the four data qubits (5, 9, 13, 16) are (4.99282, 5.08839, 5.01678, 4.96965) GHz, the two flag qubits (8, 14) are (5.20360, 5.16698) GHz, and the syndrome qubit 11 is 5.05517 GHz, respectively. The qubit anharmonicities $\alpha/2\pi$ do not vary substantially, and are approximately equal to -340 MHz.

Following Sec. III, we calibrated the SCR gates on the three qubit triplets $\{(5, 8, 9), (8, 11, 14), (13, 14, 16)\}$ found in Fig. 3(c). In advance, we also calibrated CR pulses for qubit pairs (5, 8), (9, 8), (13, 14), (16, 14), for which the default CNOT gates are implemented with CR pulses in the opposite direction. That means, for example, CNOT(5, 8) is implemented with CR(8, 5), i.e. CR drive on qubit 8 within the frame of qubit 5, while CR(5, 8) is necessary to implement SCR gate on (5, 8, 9).

We initialized the four data qubits using all possible 16 product states ranging from $|++++\rangle$ to $|----\rangle$. Here, $|+\rangle$ and $|-\rangle$ are the eigenstates of Pauli X operator. For each input state, we ran the parity check circuit 40,000 times. We scheduled circuits in an as-late-as-possible manner, where the total duration of the resulting circuits were 2261 ns (Two-CX) and 1365 ns (SCR) excluding the input state preparation and the final measurements.

We quantified how much the use of SCR gate improves the accuracy of the parity measurement by comparing the syndrome and the data error probabilities. The syndrome error probability is the probability that an incorrect bit is measured at the syndrome qubit. Here, the correct syndrome is 0 when the number of $+$ in an input state is even, and 1 when odd. The data error

probability is the probability that a state different from the input is measured at the end of a parity check circuit. Note that those values are affected by SPAM (State Preparation And Measurement) errors. As shown in Table I, the syndrome error probability averaged over all 16 initial states is significantly improved by the SCR implementation from 0.1229 down to 0.0885 ($\approx 28\%$ improvement), while the average data error rate is reduced from 0.1641 to 0.0957 ($\approx 42\%$ improvement).

We conducted the same experiment on different devices and qubits, and obtained similar results as above. For example, the average syndrome error probability was improved from 0.1566 to 0.1252 on qubits (0, 1, 2, 4, 6, 7, 10) of `ibmq_mumbai` (See Appendix 4 for more experimental results including the cases when running circuits with dynamical decoupling sequences).

V. CONCLUSION AND OUTLOOK

We have presented a pulse-level implementation of Z -parity gate with simultaneous CR drives. We have shown that this SCR implementation has little unwanted Hamiltonian terms in theory and hence it can achieve better gate fidelity than a naive implementation with CNOT gates in practice. We have also demonstrated using IBM CR devices that our calibrated parity gates significantly improve the error probability of the parity measurement for heavy-hexagon code. That suggests, as the cost of SCR gate calibration is not large, optimizing circuits using Z -parity gates can be a good option for reducing errors on superconducting quantum computing devices with all-microwave control.

Although we focused on the X -parity measurement of the heavy-hexagon code in Section IV, Z -parity gate is also naturally useful for the Z -parity measurement. Also, our method for calibrating the Z -parity gate can be extended to four- or more-qubit parity gates, which are required for other QEC code such as the surface code on a square lattice [57–61] or another LDPC code on more dense lattice [62].

TABLE I. Syndrome and data error probabilities averaged over 16 initial states of the X -parity measurement. Individual qubit date errors are described in D1–D4 columns.

	Syndrome error (std)	Data error	D1	D2	D3	D4
SCRP	0.088459 (0.001419)	0.095697	0.034948	0.031270	0.017192	0.016798
Two-CX	0.122878 (0.001639)	0.164109	0.045063	0.034634	0.066089	0.030228

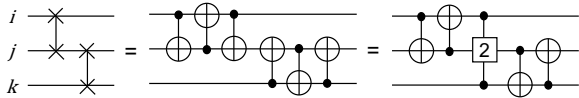


FIG. 4. Optimizing the decomposition of a chain of SWAP gates using Z -parity gates. For $N \geq 2$ successive swaps, standard decomposition requires $3N$ CNOTs. The Z -parity decomposition, however, requires $N - 1$ Z -parity, $N + 2$ CNOTs, and $O(2N)$ Hadamard gates. Assuming a similar gate time for the Z -parity and CNOT gates implemented via SCRП and ECR, the decomposition reduces the circuit depth by a factor of approximately $2/3$.

One limitation in the SCRП approach, not mentioned in Sec. IV, is that CR pulses cannot be always calibrated in all pairs of coupled qubits, e.g., due to frequency collisions in physical qubits with fixed frequencies [45, 63]. This suggests that for qubit triplets that are close to frequency collisions, tuning a SCRП gate might not be optimal. We, however, expect that improvements in manufacturing process techniques such as laser annealing [64] makes our proposal more feasible. Secondly, we have assumed that cross-drive errors in Z -parity gate with the SCRП implementation is negligible in our pulse strength regime based on the discussion in Sec. II. This assumption, however, breaks down for faster SCRП gate implementation which requires stronger drives.

It is worth noting that supporting a parity gate as a native instruction will be useful not only for improving parity measurements but also for optimizing circuits aimed for noisy quantum computers without QEC. For example, circuits with a chain of SWAP gates can be optimized using Z -parity gates. Such circuits often appear after qubit routing, which transforms a circuit to be executable on a quantum computer with limited qubit connectivity [65–68]. As a SWAP gate is symmetric and $\text{SWAP}(i, j)$ is equivalent with $\text{CNOT}(i, j) - \text{CNOT}(j, i) - \text{CNOT}(i, j)$, two consecutive SWAP gates with a common qubit, $\text{SWAP}(i, j)$ and $\text{SWAP}(j, k)$, can be decomposed into a sequence with a Z -parity gate and four CNOT gates as shown in Fig. 4. The sequence using a Z -parity gate will have a shorter circuit length than a naive sequence with six CNOT gates, and hence should have a higher fidelity.

VI. ACKNOWLEDGMENT

The authors thank Luke Govia, David Mackay, Emily Pritchett, and Xuan Wei for helpful discussions and suggestions. For the development of the analytical techniques used to derive the effective gate-operation, MM acknowledges the support of the Army Research Office under Grant Number W911NF-21-1-0002. The views and conclusions contained in this document are those of the authors and should not be interpreted as representing the official policies, either expressed or implied, of the Army Research Office or the U.S. Government. The U.S. Government is authorized to reproduce and distribute reprints for Government purposes notwithstanding any copyright notation herein.

APPENDIX

1. Calibration of rotary tone for SCRП gate

We describe how we calibrated the rotary tone on the target qubit for the SCRП implementation of a Z -parity gate. We calibrated only the amplitude of the rotary tone in this paper, however, our technique is applicable to calibrating the angle as well. We swept fifty amplitude values equally spaced between 0 and a value which corresponds to about $X_{2\pi}$ rotation, and set it to minimize the total estimated error. We defined a cost function for the error

$$\sum_{Q,R \in \{I,Z\}, P \in \{Y,Z\}} \|A_{QPR}\|,$$

where A_{QPR} denotes the coefficient of a Pauli QPR in the time evolution operator for the gate (discussed later in Eq.(13)). In the following, we explain how to estimate the cost function from experimentally available data following and generalizing the HEAT (Hamiltonian Error Amplifying Tomography) technique [30]. Note that another generalization of HEAT to capture non-Markovian off-resonant errors, not considered in this paper, is proposed in [55].

a. Echoed CR gate analysis

We first briefly recap HEAT for echoed CR gates with rotary tones to implement $ZX_{\pi/2}$ gate, following [30]. HEAT was developed to characterize the time-evolution

according to a block-diagonal Hamiltonian. In the case of echoed CR gate, the time evolution unitary operator U over the gate duration t_g can be represented in a block-diagonal Pauli basis as:

$$U = \sum_{Q \in \{I, Z\}, P \in \{I, X, Y, Z\}} A_{QP} QP. \quad (9)$$

HEAT estimates the coefficients A_{QP} from experimentally available statistics. Finally, it reconstructs the coefficients of effective Hamiltonian \tilde{H} by $\tilde{H} = i \log(U)/2t_g$. Here, we omit the last step and use the coefficients of U when using HEAT for the rotary tone calibration.

The block-diagonal form of U means that we have independent subspaces corresponding to initial control states. If the controls are in $|0\rangle$, the evolution of the target qubit is described by

$$U_{|0\rangle} = \sum_{P \in \{I, X, Y, Z\}} A_P^{(0)} P = \sum_{P \in \{I, X, Y, Z\}} (A_{IP} + A_{ZP}) P,$$

and, if the control is in $|1\rangle$, by

$$U_{|1\rangle} = \sum_{P \in \{I, X, Y, Z\}} A_P^{(1)} P = \sum_{P \in \{I, X, Y, Z\}} (A_{IP} - A_{ZP}) P.$$

The point is that A_{IP} and A_{ZP} can be reconstructed from $A_P^{(0)}$ and $A_P^{(1)}$ for any Pauli P in $\{X, Y, Z\}$ since they are related to the Walsh transform.

As $U_{|b\rangle}$ for each $b \in \{0, 1\}$ is a single qubit rotation, it can be characterized by a generic $SU(2)$ rotation around an axis given by \hat{n}_b with rotation angle θ_b :

$$U_{|b\rangle} = e^{-i(\theta_b/2)\hat{n}_b \cdot (X, Y, Z)},$$

hence, for P in $\{X, Y, Z\}$,

$$A_P^{(b)} = -i \hat{n}_{b,P} \sin\left(\frac{\theta_b}{2}\right), \quad (10)$$

where $\hat{n}_{b,P}$ denotes the P -coordinate value of \hat{n}_b .

In particular, we are interested in error terms, i.e. the cases of $P = Y$ or Z . In these cases, the right hand side of Eq. (10) can be estimated from experimentally measurable values $\text{tr}(\rho_N^{b,Y} Z)$ and $\text{tr}(\rho_N^{b,Z} Y)$ as follows:

$$\frac{\text{tr}(\rho_N^{b,Y} Z)}{N} \approx -\hat{n}_{b,Y} \sin \theta_b, \quad \frac{\text{tr}(\rho_N^{b,Z} Y)}{N} \approx \hat{n}_{b,Z} \sin \theta_b. \quad (11)$$

Here $\rho_N^{b,P}$ ($P \in \{Y, Z\}$) is the output state from even N repetitions of the echoed CR pulses with a target refocusing P , the so-called HEAT sequence, shown in Fig. 5. Moreover, $\text{tr}(\cdot Y)$ denotes measuring the target qubit in the Y basis.

From Eq. (10) and (11) with $\theta_b \approx \pm \frac{\pi}{2}$, as we are calibrating $ZX_{\pi/2}$ gate, we obtain

$$A_Y^{(b)} \approx i \frac{\text{tr}(\rho_N^{b,Y} Z)}{\sqrt{2N}}, \quad A_Z^{(b)} \approx -i \frac{\text{tr}(\rho_N^{b,Z} Y)}{\sqrt{2N}}. \quad (12)$$

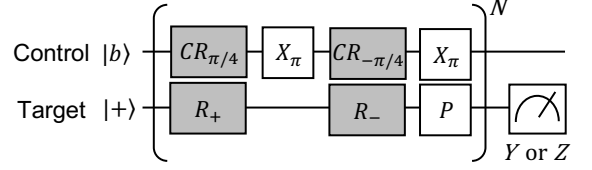


FIG. 5. HEAT sequence for echoed CR gate.

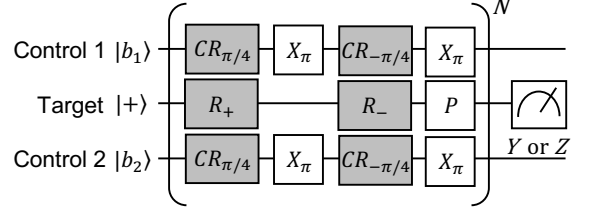


FIG. 6. HEAT sequence for echoed SCRP gate.

Intuitively, these results can be interpreted as conditional $X_{\pm\pi/2}$ rotation on the target qubit by $ZX_{\pi/2}$ interaction effectively tweaks the rotation axis of Y and Z errors by around $\pi/4$ in the YZ plane, resulting in the scale $\frac{1}{\sqrt{2}}$ for the measurement values.

b. Echoed SCRP gate analysis

In the same way, we consider a model for the echoed SCRP gate with a rotary tone to implement $ZXI_{\pi/2} + IXZ_{\pi/2}$ gate, which is locally equivalent to the Z -parity gate. Assuming a block-diagonal effective Hamiltonian with Pauli terms only in the form of QPR for $Q, R \in \{I, Z\}$ and $P \in \{I, X, Y, Z\}$, we approximate the unitary evolution as

$$U = \sum_{Q, R \in \{I, Z\}, P \in \{I, X, Y, Z\}} A_{QPR} QPR. \quad (13)$$

Note that $A_{ZII} = A_{IIZ} = 0$ since they are canceled out by echoing just as $A_{ZI} = 0$ in the echoed CR case [30].

Under the block-diagonal assumption for U , we have four blocks corresponding to the initial control bits $b \in \{00, 01, 10, 11\}$:

$$U_{|b\rangle} = \sum_{P \in \{I, X, Y, Z\}} A_P^{(b)} P, \quad (14)$$

where

$$\begin{aligned} A_P^{(00)} &= A_{IPI} + A_{ZPI} + A_{IPZ} + A_{ZPZ}, \\ A_P^{(10)} &= A_{IPI} - A_{ZPI} + A_{IPZ} - A_{ZPZ}, \\ A_P^{(01)} &= A_{IPI} + A_{ZPI} - A_{IPZ} - A_{ZPZ}, \\ A_P^{(11)} &= A_{IPI} - A_{ZPI} - A_{IPZ} + A_{ZPZ}. \end{aligned}$$

Again, A_{PI} , A_{ZPI} , A_{IPZ} and A_{ZPZ} can be reconstructed from $A_P^{(00)}$, $A_P^{(10)}$, $A_P^{(01)}$, $A_P^{(11)}$ for any Pauli P in $\{X, Y, Z\}$ as they are related with the Walsh transform. Also, similar relations hold as in Eq. (10) for $b \in \{00, 01, 10, 11\}$.

In contrast, the relationship between experimentally measurable values and the axis of target rotation \hat{n}_b is slightly different as follows. In the case of $b \in \{01, 10\}$, i.e. $\theta_b \approx 0$,

$$\frac{\text{tr}(\rho_N^{b,Y} Z)}{N} \approx -2\hat{n}_{b,Y}, \quad \frac{\text{tr}(\rho_N^{b,Z} Y)}{N} \approx 2\hat{n}_{b,Z}, \quad (15)$$

while, in the case of b is 00 or 11, i.e. $\theta_b \approx \pi$ or $-\pi$,

$$\frac{\text{tr}(\rho_N^{b,Y} Y)}{N} \approx -2\hat{n}_{b,Y}, \quad \frac{\text{tr}(\rho_N^{b,Z} Z)}{N} \approx -2\hat{n}_{b,Z}. \quad (16)$$

Here $\rho_N^{b,P}$ ($P \in \{Y, Z\}$) is the output state of the HEAT sequence for echoed SCRP gate with input bits b for the control qubits as shown in Fig. 6. Consequently, for $b \in \{01, 10\}$, we have

$$A_Y^{(b)} \approx i \frac{\text{tr}(\rho_N^{b,Y} Z)}{2N}, \quad A_Z^{(b)} \approx -i \frac{\text{tr}(\rho_N^{b,Z} Y)}{2N}, \quad (17)$$

that means we can see Y (Z) rotation errors in Z (Y) basis as in the case of CR gate. However, for the case of $b \in \{00, 11\}$, we have

$$A_Y^{(00)} \approx i \frac{\text{tr}(\rho_N^{00,Y} Y)}{2N}, \quad A_Z^{(00)} \approx i \frac{\text{tr}(\rho_N^{00,Z} Z)}{2N}, \quad (18)$$

$$A_Y^{(11)} \approx -i \frac{\text{tr}(\rho_N^{11,Y} Y)}{2N}, \quad A_Z^{(11)} \approx -i \frac{\text{tr}(\rho_N^{11,Z} Z)}{2N}, \quad (19)$$

that suggests we need to measure in the Y (Z) basis in order to see Y (Z) rotation errors in contrast to the case of CR gate. Those can be explained by the effect of desirable $ZXI_{\pi/2} + IXZ_{\pi/2}$ interaction on the errors on the target qubit. For example, if the control qubits are in the $|00\rangle$ state ($b = 00$), the desirable interaction rotate the target qubit by π around X axis, that tweaks the rotation axis of Y and Z errors by $\pi/2$ in the YZ plane, changing the axes on which the errors appears.

2. Three-qubit Randomized benchmarking

We describe how to prepare circuits for three-qubit RB. As we are considering the physical implementation of Z -parity gates, we are interested in RB on qubit triplets on a line (i, j, k) . That suggests CNOT gates are natively supported on qubits $\{i, j\}$ and $\{j, k\}$ in a device, but not on qubits $\{i, k\}$. Typically, RB circuits are constructed from sequences of Clifford operations. We construct the circuits in two steps. We first decompose three-qubit Cliffords into basic one- or two-qubit instructions, e.g. Rz,

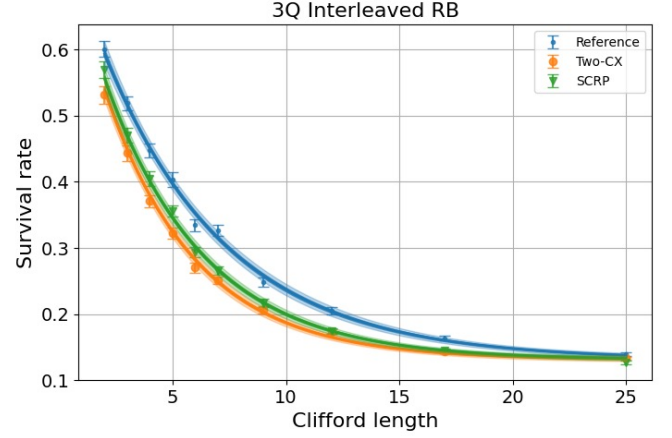


FIG. 7. Interleaved RB of Z -parity gate on qubits (5, 8, 9) in `ibm_auckland`. The estimated EPGs are 0.0540 ± 0.0034 (Two-CX) and 0.0369 ± 0.0032 (SCRP).

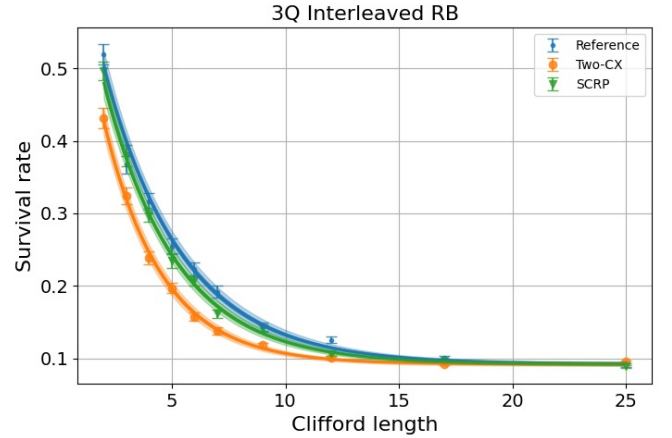


FIG. 8. Interleaved RB of Z -parity gate on qubits (13, 14, 16) in `ibm_auckland`. The estimated EPGs are 0.0839 ± 0.0059 (Two-CX) and 0.0231 ± 0.0054 (SCRP).

SX and CNOT for `ibm_auckland`, without considering the connectivity of qubits. Then, if we have any CNOT gates on not directly connected qubits $\{i, k\}$, we decompose them further into the sequence of four CNOT gates: $\text{CNOT}(i, k)$ into a sequence $\text{CNOT}(j, k) - \text{CNOT}(i, j) - \text{CNOT}(j, k) - \text{CNOT}(i, j)$, and similarly for $\text{CNOT}(k, i)$.

In the main text, we showed the IRB result on qubits (8, 11, 14) of `ibm_auckland`. We conducted the IRB experiments on two different triplets of qubits; (5, 8, 9) and (13, 14, 16), using the same configurations except for slightly different Clifford lengths: 2, 3, 4, 5, 6, 7, 9, 12, 17, 25. The results are shown in Fig. 7 and 8, respectively.

3. Coherence limit

The *coherence limit* is an estimate of the minimum average error, which can be calculated from the gate

TABLE II. Syndrome error rates and data error rates by Z -parity gate implementation in X -parity measurement with and without dynamical decoupling (DD) for different qubits and systems.

Qubits (5, 8, 9, 11, 13, 14, 16) on <code>ibm_auckland</code>						
	Syndrome error (std)	Data error	D1	D2	D3	D4
SCRP	0.088459 (0.001419)	0.095697	0.034948	0.031270	0.017192	0.016798
SCRP (w/DD)	0.084689 (0.001392)	0.097259	0.039488	0.026717	0.018634	0.017116
Two-CX	0.122878 (0.001639)	0.164109	0.045063	0.034634	0.066089	0.030228
Two-CX (w/DD)	0.119409 (0.001620)	0.154578	0.043534	0.020895	0.065419	0.035731
Qubits (0, 1, 2, 4, 6, 7, 10) on <code>ibmq_mumbai</code>						
	Syndrome error (std)	Data error	D1	D2	D3	D4
SCRP	0.125220 (0.001636)	0.129978	0.044998	0.022061	0.023623	0.046205
SCRP (w/DD)	0.117958 (0.001594)	0.123977	0.045114	0.018409	0.023853	0.042817
Two-CX	0.156625 (0.001806)	0.182667	0.053606	0.045355	0.031783	0.065836
Two-CX (w/DD)	0.120066 (0.001609)	0.139727	0.051256	0.023038	0.026319	0.047777

length and experimentally measurable noise indicators of each qubit, i.e. energy relaxation (T_1) and dephasing (T_2) times [54, 55, 69]. It provides a rough lower bound on average gate error in the case when we could implement a gate perfectly on imperfect qubits, assuming only gate-independent single-qubit amplitude damping and dephasing channels.

The coherence limit is formally defined as a spacial case of the average gate infidelity of a gate U under the above assumption on noises:

$$1 - F_{\text{avg}}(\Lambda(U), U) = \frac{d}{d+1} \left(1 - \frac{\text{tr}[S_\Lambda]}{d^2} \right) = \frac{d}{d+1} \left(1 - \prod_{q \in Q} \text{tr}[S_{\Lambda_q}] \right), \quad (20)$$

where $\Lambda(U)$ is the quantum channel representing a noisy realization of U , $d = 2^n$ is the dimension of Hilbert space of n -qubit system (denoted by Q), S_Λ denotes the Pauli superoperator (or Pauli Transfer Matrix, PTM) representation of the channel Λ , $F_{\text{avg}}(\mathcal{E}, U)$ is the average gate fidelity between a quantum channel \mathcal{E} and a unitary channel U . The first equality in Eq.(20) is obtained from the gate-independence of noises. In general, the average gate infidelity and the process (or entanglement) infidelity are related to

$$1 - F_{\text{avg}}(\Lambda(U), U) = \frac{d}{d+1} (1 - F_{\text{pro}}(\Lambda(U), U)).$$

And, for the gate-independent noise channel Λ , we can rewrite those without U since we have $S_{\Lambda(U)} = S_\Lambda S_U$, hence

$$F_{\text{pro}}(\Lambda(U), U) = \frac{\text{tr}[S_U^\dagger S_{\Lambda(U)}]}{d^2} = \frac{\text{tr}[S_\Lambda]}{d^2}.$$

The second equality in Eq.(20) is obtained from the qubit-independence of noises, that allows

$$\text{tr}[S_\Lambda] = \text{tr} \left[\bigotimes_{q \in Q} S_{\Lambda_q} \right] = \prod_{q \in Q} \text{tr}[S_{\Lambda_q}].$$

Recalling the third assumption, that the single-qubit noise Λ_q is an amplitude-phase damping channel, we can explicitly write down the PTM as

$$S_{\Lambda_q} = \begin{bmatrix} 1 & 0 & 0 & 0 \\ 0 & e^{-\frac{t}{T_2(q)}} & 0 & 0 \\ 0 & 0 & e^{-\frac{t}{T_2(q)}} & 0 \\ 1 - e^{-\frac{t}{T_1(q)}} & 0 & 0 & e^{-\frac{t}{T_1(q)}} \end{bmatrix} \quad (21)$$

with the gate length t and the T_1 and the T_2 value, $T_1(q)$ and $T_2(q)$, for each $q \in Q$. Consequently, we can compute the coherence limit based on Eq.(20) and (21).

4. Experiments with dynamical decoupling

We examined how the results of X -parity measurement experiments discussed in Section IV are affected by applying dynamical decoupling (DD) [70–72]. We performed exactly the same X -parity check circuits as described in Section IV, except for DD on qubits during their idling time. The DD sequence we applied was one of the simplest, Delay(τ)- $X_{+\pi}$ -Delay(2τ)- $X_{-\pi}$ -Delay(τ) with $\tau \geq 0$.

As shown in Table II, the effect of DD depends on qubits in use and the implementation of Z -parity gates. For qubits (5, 8, 9, 11, 13, 14, 16) on `ibm_auckland`, there is no improvement in the figures of merit for SCRIP implementation while there is slight improvement in data error (around 1%) for Two-CX implementation. This is not surprising as DD does not always improve the circuit fidelity as discussed in [73]. In contrast, for qubits (0, 1, 2, 4, 6, 7, 10) on `ibmq_mumbai`, DD improves performance for both SCRIP and Two-CX implementation. The syndrome error is decreased by around 0.7% for SCRIP and 3.6% for Two-CX. The data error is decreased by around 0.6% for SCRIP and 4.3% for Two-CX. DD tends to improve performance more for Two-CX implementation than for SCRIP. However, even after the application of DD, SCRIP implementation still performs better than Two-CX implementation. For example, for qubits (5, 8,

9, 11, 13, 14, 16) on `ibm_auckland`, SCRP implementation with DD improved the syndrome error rate from 0.1194 to 0.0847 ($\approx 29\%$ improvement) comparing with

Two-CX implementation with DD while it improved the data error rate from 0.1546 to 0.0973 ($\approx 37\%$ improvement).

-
- [1] Michael A Nielsen and Isaac L Chuang. Quantum computation and quantum information. *Phys. Today*, 54(2):60, 2001.
- [2] Alexei Yu Kitaev, Alexander Shen, and Mikhail N Vyalyi. *Classical and quantum computation*. Number 47. American Mathematical Soc., 2002.
- [3] Adriano Barenco, Charles H Bennett, Richard Cleve, David P DiVincenzo, Norman Margolus, Peter Shor, Tychon Sleator, John A Smolin, and Harald Weinfurter. Elementary gates for quantum computation. *Physical review A*, 52(5):3457, 1995.
- [4] Crispin Gardiner and Peter Zoller. *Quantum noise: a handbook of Markovian and non-Markovian quantum stochastic methods with applications to quantum optics*. Springer Science & Business Media, 2004.
- [5] Aashish A Clerk, Michel H Devoret, Steven M Girvin, Florian Marquardt, and Robert J Schoelkopf. Introduction to quantum noise, measurement, and amplification. *Reviews of Modern Physics*, 82(2):1155, 2010.
- [6] Philip Krantz, Morten Kjaergaard, Fei Yan, Terry P Orlando, Simon Gustavsson, and William D Oliver. A quantum engineer’s guide to superconducting qubits. *Applied physics reviews*, 6(2), 2019.
- [7] Dmitri Maslov, Christina Young, D Michael Miller, and Gerhard W Dueck. Quantum circuit simplification using templates. In *Design, Automation and Test in Europe*, pages 1208–1213. IEEE, 2005.
- [8] Dmitri Maslov, Gerhard W Dueck, D Michael Miller, and Camille Negrevergne. Quantum circuit simplification and level compaction. *IEEE Transactions on Computer-Aided Design of Integrated Circuits and Systems*, 27(3):436–444, 2008.
- [9] Vadym Kliuchnikov, Dmitri Maslov, and Michele Mosca. Asymptotically optimal approximation of single qubit unitaries by Clifford and T circuits using a constant number of ancillary qubits. *Physical review letters*, 110(19):190502, 2013.
- [10] Matthew Amy, Dmitri Maslov, and Michele Mosca. Polynomial-time T-depth optimization of Clifford+T circuits via matroid partitioning. *IEEE Transactions on Computer-Aided Design of Integrated Circuits and Systems*, 33(10):1476–1489, 2014.
- [11] Yunseong Nam, Neil J Ross, Yuan Su, Andrew M Childs, and Dmitri Maslov. Automated optimization of large quantum circuits with continuous parameters. *npj Quantum Information*, 4(1):23, 2018.
- [12] Guido Burkard, Daniel Loss, David P DiVincenzo, and John A Smolin. Physical optimization of quantum error correction circuits. *Physical Review B*, 60(16):11404, 1999.
- [13] Anders Sørensen and Klaus Mølmer. Entanglement and quantum computation with ions in thermal motion. *Physical Review A*, 62(2):022311, 2000.
- [14] Arkady Fedorov, Lars Steffen, Matthias Baur, Marcus P da Silva, and Andreas Wallraff. Implementation of a Toffoli gate with superconducting circuits. *Nature*, 481(7380):170–172, 2012.
- [15] Esteban A Martinez, Thomas Monz, Daniel Nigg, Philipp Schindler, and Rainer Blatt. Compiling quantum algorithms for architectures with multi-qubit gates. *New Journal of Physics*, 18(6):063029, 2016.
- [16] Wei Feng and Da-wei Wang. Quantum Fredkin gate based on synthetic three-body interactions in superconducting circuits. *Physical Review A*, 101(6):062312, 2020.
- [17] Marie Lu, Jean-Loup Ville, Joachim Cohen, Alexandru Petrescu, Sydney Schreppler, Larry Chen, Christian Jünger, Chiara Pelletti, Alexei Marchenkov, Archan Banerjee, et al. Multipartite entanglement in Rabi-Driven superconducting qubits. *PRX Quantum*, 3(4):040322, 2022.
- [18] Xiu Gu, Jorge Fernández-Pendás, Pontus Vikstål, Tahereh Abad, Christopher Warren, Andreas Bengtsson, Giovanna Tancredi, Vitaly Shumeiko, Jonas Bylander, Göran Johansson, et al. Fast multiqubit gates through simultaneous two-qubit gates. *PRX Quantum*, 2(4):040348, 2021.
- [19] Christopher W Warren, Jorge Fernández-Pendás, Shahnawaz Ahmed, Tahereh Abad, Andreas Bengtsson, Janka Biznárová, Kamanasish Debnath, Xiu Gu, Christian Križan, Amr Osman, et al. Extensive characterization and implementation of a family of three-qubit gates at the coherence limit. *npj Quantum Information*, 9(1):44, 2023.
- [20] Yosep Kim, Alexis Morvan, Long B Nguyen, Ravi K Naik, Christian Jünger, Larry Chen, John Mark Kreikebaum, David I Santiago, and Irfan Siddiqi. High-fidelity three-qubit iToffoli gate for fixed-frequency superconducting qubits. *Nature Physics*, 18(7):783–788, 2022.
- [21] GS Paraoanu. Microwave-induced coupling of superconducting qubits. *Physical Review B*, 74(14):140504, 2006.
- [22] Chad Rigetti and Michel Devoret. Fully microwave-tunable universal gates in superconducting qubits with linear couplings and fixed transition frequencies. *Physical Review B*, 81(13):134507, 2010.
- [23] Vinay Tripathi, Mostafa Khezri, and Alexander N. Korotkov. Operation and intrinsic error budget of a two-qubit cross-resonance gate. *Phys. Rev. A*, 100:012301, Jul 2019.
- [24] Easwar Magesan and Jay M Gambetta. Effective Hamiltonian models of the cross-resonance gate. *Physical Review A*, 101(5):052308, 2020.
- [25] Moein Malekakhlagh, Easwar Magesan, and David C McKay. First-principles analysis of cross-resonance gate operation. *Phys. Rev. A*, 102:042605, Oct 2020.
- [26] In this term, three-qubit refers gate (not parity), in fact, TP gate checks two-qubit parity.
- [27] Antonio D Córcoles, Jay M Gambetta, Jerry M Chow, John A Smolin, Matthew Ware, Joel Strand, Britton LT Plourde, and Matthias Steffen. Process verification of two-qubit quantum gates by randomized benchmarking. *Physical Review A*, 87(3):030301, 2013.
- [28] Sarah Sheldon, Easwar Magesan, Jerry M. Chow, and

- Jay M. Gambetta. Procedure for systematically tuning up crosstalk in the cross resonance gate. *Physical Review A*, 93, 3 2016.
- [29] Petar Jurcevic, Ali Javadi-Abhari, Lev S Bishop, Isaac Lauer, Daniela F Bogorin, Markus Brink, Lauren Capeluto, Oktay Günlük, Toshinari Itoko, Naoki Kanazawa, et al. Demonstration of quantum volume 64 on a superconducting quantum computing system. *Quantum Science and Technology*, 6(2):025020, 2021.
- [30] Neereja Sundaresan, Isaac Lauer, Emily Pritchett, Easwar Magesan, Petar Jurcevic, and Jay M Gambetta. Reducing unitary and spectator errors in cross resonance with optimized rotary echoes. *PRX Quantum*, 1(2):020318, 2020.
- [31] Matthew J Reagor, Thomas C Bohdanowicz, David Rodriguez Perez, Eyob A Sete, and William J Zeng. Hardware optimized parity check gates for superconducting surface codes. *arXiv preprint arXiv:2211.06382*, 2022.
- [32] K Dodge, Y Liu, AR Klots, B Cole, A Shearrow, M Senatore, S Zhu, LB Ioffe, R McDermott, and BLT Plourde. Hardware implementation of quantum stabilizers in superconducting circuits. *arXiv preprint arXiv:2303.00625*, 2023.
- [33] Daniel M Greenberger, Michael A Horne, and Anton Zeilinger. Going beyond Bell’s theorem. In *Bell’s theorem, quantum theory and conceptions of the universe*, pages 69–72. Springer, 1989.
- [34] Dik Bouwmeester, Jian-Wei Pan, Matthew Daniell, Harald Weinfurter, and Anton Zeilinger. Observation of three-photon Greenberger-Horne-Zeilinger entanglement. *Physical Review Letters*, 82(7):1345, 1999.
- [35] Peter W Shor. Scheme for reducing decoherence in quantum computer memory. *Physical review A*, 52(4):R2493, 1995.
- [36] A Robert Calderbank and Peter W Shor. Good quantum error-correcting codes exist. *Physical Review A*, 54(2):1098, 1996.
- [37] Barbara M Terhal. Quantum error correction for quantum memories. *Reviews of Modern Physics*, 87(2):307, 2015.
- [38] Seth Lloyd. A potentially realizable quantum computer. *Science*, 261(5128):1569–1571, 1993.
- [39] David P DiVincenzo, Dave Bacon, Julia Kempe, Guido Burkard, and K Birgitta Whaley. Universal quantum computation with the exchange interaction. *nature*, 408(6810):339–342, 2000.
- [40] Neereja Sundaresan, Theodore J. Yoder, Youngseok Kim, Muyuan Li, Edward H. Chen, Grace Harper, Ted Thorbeck, Andrew W. Cross, Antonio D. Córcoles, and Maika Takita. Matching and maximum likelihood decoding of a multi-round subsystem quantum error correction experiment. 3 2022.
- [41] The ordering of qubits is (control-0, target, control-1) throughout this paper.
- [42] John R Schrieffer and Peter A Wolff. Relation between the Anderson and Kondo Hamiltonians. *Physical Review*, 149(2):491, 1966.
- [43] Moein Malekakhlagh and Easwar Magesan. Mitigating off-resonant error in the cross-resonance gate. *Phys. Rev. A*, 105:012602, Jan 2022.
- [44] Moein Malekakhlagh, Easwar Magesan, and Luke CG Govia. Time-dependent Schrieffer-Wolff-Lindblad perturbation theory: Measurement-induced dephasing and second-order stark shift in dispersive readout. *Physical Review A*, 106(5):052601, 2022.
- [45] Kentaro Heya, Moein Malekakhlagh, Seth Merkel, Naoki Kanazawa, and Emily Pritchett. Floquet analysis of frequency collisions. *arXiv preprint arXiv:2302.12816*, 2023.
- [46] Joseph Emerson, Robert Alicki, and Karol Życzkowski. Scalable noise estimation with random unitary operators. *Journal of Optics B: Quantum and Semiclassical Optics*, 7(10):S347, 2005.
- [47] Emanuel Knill, Dietrich Leibfried, Rolf Reichle, Joe Britton, R Brad Blakestad, John D Jost, Chris Langer, Roee Ozeri, Signe Seidelin, and David J Wineland. Randomized benchmarking of quantum gates. *Physical Review A*, 77(1):012307, 2008.
- [48] Easwar Magesan, Jay M Gambetta, and Joseph Emerson. Scalable and robust randomized benchmarking of quantum processes. *Physical review letters*, 106(18):180504, 2011.
- [49] Easwar Magesan, Jay M Gambetta, Blake R Johnson, Colm A Ryan, Jerry M Chow, Seth T Merkel, Marcus P Da Silva, George A Keefe, Mary B Rothwell, Thomas A Ohki, et al. Efficient measurement of quantum gate error by interleaved randomized benchmarking. *Physical review letters*, 109(8):080505, 2012.
- [50] IBM Quantum. <https://quantum-computing.ibm.com/>, 2023.
- [51] Christopher Chamberland, Guanyu Zhu, Theodore J Yoder, Jared B Hertzberg, and Andrew W Cross. Topological and subsystem codes on low-degree graphs with flag qubits. *Physical Review X*, 10(1):011022, 2020.
- [52] Edward H Chen, Theodore J Yoder, Youngseok Kim, Neereja Sundaresan, Srikanth Srinivasan, Muyuan Li, Antonio D Córcoles, Andrew W Cross, and Maika Takita. Calibrated decoders for experimental quantum error correction. *Physical Review Letters*, 128(11):110504, 2022.
- [53] Neereja Sundaresan, Theodore J Yoder, Youngseok Kim, Muyuan Li, Edward H Chen, Grace Harper, Ted Thorbeck, Andrew W Cross, Antonio D Córcoles, and Maika Takita. Demonstrating multi-round subsystem quantum error correction using matching and maximum likelihood decoders. *Nature Communications*, 14(1):2852, 2023.
- [54] Jay M Gambetta, Antonio D Córcoles, Seth T Merkel, Blake R Johnson, John A Smolin, Jerry M Chow, Colm A Ryan, Chad Rigetti, Stefano Poletto, Thomas A Ohki, et al. Characterization of addressability by simultaneous randomized benchmarking. *Physical review letters*, 109(24):240504, 2012.
- [55] Ken Xuan Wei, Emily Pritchett, David M Zajac, David C McKay, and Seth Merkel. Characterizing non-markovian off-resonant errors in quantum gates. *arXiv preprint arXiv:2302.10881*, 2023.
- [56] Edward H. Chen, Theodore J. Yoder, Youngseok Kim, Neereja Sundaresan, Srikanth Srinivasan, Muyuan Li, Antonio D. Córcoles, Andrew W. Cross, and Maika Takita. Calibrated decoders for experimental quantum error correction. 10 2021.
- [57] Sergey B Bravyi and A Yu Kitaev. Quantum codes on a lattice with boundary. *arXiv preprint quant-ph/9811052*, 1998.
- [58] Eric Dennis, Alexei Kitaev, Andrew Landahl, and John Preskill. Topological quantum memory. *Journal of Mathematical Physics*, 43(9):4452–4505, 2002.
- [59] Alexei Kitaev. Anyons in an exactly solved model and beyond. *Annals of Physics*, 321(1):2–111, 2006.
- [60] Austin G Fowler, Ashley M Stephens, and Peter

- Groszkowski. High-threshold universal quantum computation on the surface code. *Physical Review A*, 80(5):052312, 2009.
- [61] Austin G Fowler, Matteo Mariantoni, John M Martinis, and Andrew N Cleland. Surface codes: Towards practical large-scale quantum computation. *Physical Review A*, 86(3):032324, 2012.
- [62] Sergey Bravyi, Andrew W Cross, Jay M Gambetta, Dmitri Maslov, Patrick Rall, and Theodore J Yoder. High-threshold and low-overhead fault-tolerant quantum memory. *arXiv preprint arXiv:2308.07915*, 2023.
- [63] Jared B Hertzberg, Eric J Zhang, Sami Rosenblatt, Easwar Magesan, John A Smolin, Jeng-Bang Yau, Vivekananda P Adiga, Martin Sandberg, Markus Brink, Jerry M Chow, et al. Laser-annealing Josephson junctions for yielding scaled-up superconducting quantum processors. *npj Quantum Information*, 7(1):129, 2021.
- [64] Eric J Zhang, Srikanth Srinivasan, Neereja Sundaresan, Daniela F Bogorin, Yves Martin, Jared B Hertzberg, John Timmerwilke, Emily J Pritchett, Jeng-Bang Yau, Cindy Wang, et al. High-performance superconducting quantum processors via laser annealing of transmon qubits. *Science Advances*, 8(19):eabi6690, 2022.
- [65] Alwin Zulehner, Alexandru Paler, and Robert Wille. An efficient methodology for mapping quantum circuits to the IBM QX architectures. *IEEE Transactions on Computer-Aided Design of Integrated Circuits and Systems*, 38(7):1226–1236, 2018.
- [66] Gushu Li, Yufei Ding, and Yuan Xie. Tackling the qubit mapping problem for NISQ-era quantum devices. In *Proceedings of the Twenty-Fourth International Conference on Architectural Support for Programming Languages and Operating Systems*, pages 1001–1014, 2019.
- [67] Toshinari Itoko, Rudy Raymond, Takashi Imamichi, and Atsushi Matsuo. Optimization of quantum circuit mapping using gate transformation and commutation. *Integration*, 70:43–50, 2020.
- [68] Elisa Bäumer, Vinay Tripathi, Derek S Wang, Patrick Rall, Edward H Chen, Swarnadeep Majumder, Alireza Seif, and Zlatko K Minev. Efficient long-range entanglement using dynamic circuits. *arXiv preprint arXiv:2308.13065*, 2023.
- [69] Tahereh Abad, Jorge Fernández-Pendás, Anton Frisk Kockum, and Göran Johansson. Universal fidelity reduction of quantum operations from weak dissipation. *Physical Review Letters*, 129(15):150504, 2022.
- [70] Lorenza Viola, Emanuel Knill, and Seth Lloyd. Dynamical decoupling of open quantum systems. *Physical Review Letters*, 82(12):2417, 1999.
- [71] Alexandre M Souza, Gonzalo A Alvarez, and Dieter Suter. Robust dynamical decoupling for quantum computing and quantum memory. *Physical review letters*, 106(24):240501, 2011.
- [72] Dieter Suter and Gonzalo A Álvarez. Colloquium: Protecting quantum information against environmental noise. *Reviews of Modern Physics*, 88(4):041001, 2016.
- [73] Poulami Das, Swamit Tammu, Siddharth Dangwal, and Moinuddin Qureshi. Adapt: Mitigating idling errors in qubits via adaptive dynamical decoupling. In *MICRO-54: 54th Annual IEEE/ACM International Symposium on Microarchitecture*, pages 950–962, 2021.